Multiple Grazing Angle Sea Clutter Modeling

Ali Karimian, Caglar Yardim, *Member, IEEE*, Peter Gerstoft, William S. Hodgkiss, *Member, IEEE*, and Amalia E. Barrios

***Abstract*—Radar clutter in a non-standard atmosphere usually is modeled based on a single grazing angle at each range. Instead, the angular distribution of incident power can be used to obtain a more accurate model of the clutter. Angular spectral estimation provides the grazing angle distribution of propagating power. However, a large gradient in the refractivity profile, e.g., an evaporation duct, distorts plane wave propagation which in turn violates assumptions of plane wave spectral estimation. Ray tracing is used in these situations, but has its own limitations (e.g., shadow zones). We suggest using curved wave spectral estimation (CWS) that yields reliable results for any refractivity profile, in contrast to plane wave spectral estimation. CWS is used to derive multiple grazing angle clutter, a model for ocean surface clutter in the microwave region that depends on all incident angles at each range and their corresponding powers.**

***Index Terms*—Angle of arrival, angular spectral estimation, array signal processing, clutter, electromagnetics, grazing angle, parabolic wave equation, propagation, ray tracing.**

I. Introduction

LOWER atmospheric ducts over the ocean are common in many maritime regions of the world. These non-standard conditions result in effects such as significant variations in the maximum operational radar range, creation of radar fades where the radar performance is reduced, and increased sea clutter [1]. Atmospheric ducts are more common in hot and humid regions of the world. The Persian Gulf, the Mediterranean and California coasts are examples of such regions where an increase in the humidity pattern above the sea surface is accompanied by an increase in the temperature profile [2].

Calculation of the expected sea clutter power at low grazing angles requires modeling of ocean radar reflectivity per unit area [1]. It is common in practice to use the semi-empirical sea reflectivity model from the Georgia Institute of Technology (GIT) [3]. The GIT model is based on fitting a single grazing angle model to low angle sea surface clutter measurements. Dockery and Reilly modified the GIT model to take into account the effects of non-standard ducting conditions on clutter [4], [5]. They divided the GIT reflectivity by the propagation factor obtained under standard conditions to remove the standard atmosphere effect on the measurements. More recent empirical models of sea clutter at low grazing angles are investigated in [6].

The occurrence of ducting conditions causes grazing angles to be range-dependent, as the electromagnetic wave is trapped inside the duct. The strong dependence of sea surface reflectivity on low grazing angles makes estimation of these angles important. Ray tracing is a common way of finding the grazing angle at the sea surface in the microwave region. However, it fails to account for shadow zones [7]. Hence, angular spectral estimation can be used to obtain the angle of arrival (AOA) as a function of range. Vertical arrays at each range can be generated synthetically with samples of the field obtained from a parabolic equation code [8].

Grazing angle calculation in existing propagation software packages depends on tropospheric conditions. The Advanced Propagation Model (APM) software [7] uses the maximum grazing angle obtained from ray tracing for propagation over the ocean, while plane wave spectral estimation (PWS) is used to calculate the dominant grazing angle over land. The Tropospheric electromagnetic parabolic equation routine (Temper) [9] uses the MUSIC algorithm [10] in its automatic mode to obtain the grazing angle when changes of the refractivity index are high. A forward/backward spatial smoothing MUSIC method [11] is used, which divides the synthetic array into overlapping sub-arrays. This method assumes a constant refractivity along the array. Temper uses ray tracing for evaporation ducts where MUSIC is not reliable. Switching between ray tracing and spectral estimation requires an ad hoc decision rule based on the gradient of the refractivity index along the array [12], [13].

Both APM and Temper use a parabolic equation approximation to the wave equation [7], [9]. There also have been attempts to incorporate a grazing angle dependent impedance of the horizontal reflecting surface into the forward propagation formulation of the parabolic equation [14].

In this paper we propose a self-consistent way of obtaining the grazing angles so that it is not necessary to switch between grazing angle computation techniques. Curved wave spectral estimation (CWS) can be applied as an angular spectral estimation technique when the approximation of a constant refractivity index along the array fails. Hence, CWS is applicable to all atmospheric conditions with a refractivity index that varies with height.

The worst case clutter can be estimated using the maximum grazing angle obtained from ray tracing or angular spectral estimation [7]. However, a more realistic clutter model is needed in applications such as refractivity from clutter (RFC) [15]–[21]. Multiple grazing angle clutter provides such a model that takes all incident angles into account.

Manuscript received March 14, 2011; revised March 06, 2012; accepted April 09, 2012. Date of publication July 03, 2012; date of current version August 30, 2012. This work was supported by SPAWAR under Grants N66001-03-2-8938, TDL 0049 and TDL 0054.

A. Karimian is with the Department of Electrical and Computer Engineering, University of California San Diego, CA 92093 USA (e-mail: karimian@ucsd.edu).

C. Yardim, P. Gerstoft, and W. S. Hodgkiss are with Marine Physical Laboratory, Scripps Institute of Oceanography, University of California San Diego, CA 92093 USA.

A. E. Barrios is with Atmospheric Propagation Branch, Space and Naval Warfare Systems Center, San Diego, California, CA 92152 USA.

Color versions of one or more of the figures in this paper are available online at http://ieeexplore.ieee.org.

Digital Object Identifier 10.1109/TAP.2012.2207033

The single angle clutter equation is reviewed in Section II. Array processing and the effects of vertical variations of refractivity on angular spectral estimation is discussed in Section III. The angular power spectrum of the incident electromagnetic wave is used in Section IV to construct a multiple angle clutter model. Section V provides several examples to show the performance of curved wave spectral estimation and the multiple grazing angle clutter model.

II. Sea Clutter at Low Grazing Angles

Radars operating in maritime environments encounter a back-scattered signal from the sea surface. Received clutter depends on the refractivity profile of the environment known as the M-profile. This dependence makes inference of the refractivity profile from the observed clutter possible [15]. The expected clutter is expressed as [4]

$$P_c(r) = \frac{P_t G^2 \lambda^2 \theta_B c\tau \sigma_0 \sec(\theta) F^4(r)}{2(4\pi r)^3 L} \tag{1}$$

where P_t is the transmitter power, G is the antenna gain, λ is the wavelength, θ_B is the antenna pattern azimuthal beamwidth, c is the propagation speed, τ is the pulse width, σ_0 is the sea surface reflectivity per unit area, θ is the grazing angle at range r, F is the propagation factor, and L is the total assumed system losses.

The propagation factor, F, is defined as the ratio of the magnitude of the electric field at a given point under specified conditions to the magnitude of the electric field under free-space conditions with the beam of the transmitter directed toward the point in question [1]: $F(r) = |(E(r))/(E_{fs}(r))|$.

A. Modified GIT Model

The standard GIT model, see Appendix A, is a semi-empirical model that calculates the sea surface reflectivity [4]. This model is based on fitting the experimental measured average sea surface reflectivity to a function of polarization, radar frequency, grazing angle, wind speed and radar look direction. The effect of standard atmosphere can be removed by normalizing the GIT cross-section with respect to the 4/3 effective earth radius propagation factor in standard conditions [4], [22]

$$\sigma_0(r,\theta) = \frac{\sigma_{0,\mathrm{GIT}}(r,\theta)}{F^4_{\mathrm{std}}(r')} \tag{2}$$

where $F^4_{\mathrm{std}}(r')$ is the two-way propagation factor of the standard atmosphere ($(dM)/(dh) = 0.118$ M-units/m) at the equivalent range r' with the same wind speed and an isotropic antenna. r' is the range that yields the same grazing angle θ under the standard atmospheric condition [22]

$$r'(\theta) = \sqrt{a_e^2\theta^2 + 2a_e h_{\mathrm{ant}}} - a_e\theta \tag{3}$$

where a_e is the 4/3 average earth radius in meters, and h_{ant} is the antenna height relative to the sea surface.

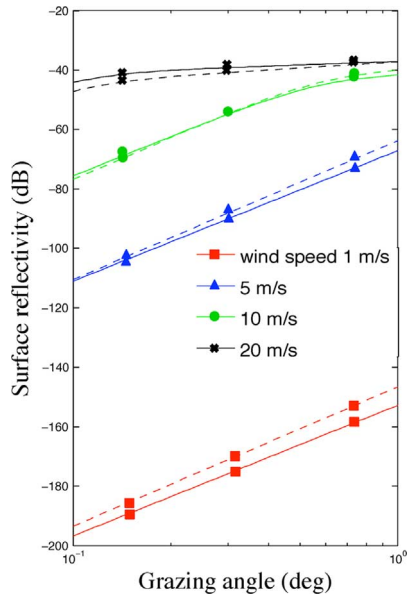

Fig. 1. The sensitivity of GIT reflectivity per unit area $\sigma_{0,\mathrm{GIT}}$ to grazing angle and wind speed at 3 GHz for horizontal (solid) and vertical (dashed) polarization.

Substitution of (2) into (1) yields the final form of the clutter power equation based on the modified GIT reflectivity

$$P_c(r) = \frac{P_t G^2 \lambda^2 \theta_B c\tau \sigma_{0,\mathrm{GIT}}(r,\theta) \sec(\theta) F^4(r)}{2(4\pi r)^3 L F^4_{\mathrm{std}}(r')}. \tag{4}$$

Fig. 1 shows changes of sea surface reflectivity per unit area $\sigma_{0,\mathrm{GIT}}$ for horizontal and vertical polarizations as a function of grazing angle and wind speed, with radar operating frequency of 3 GHz. Note that σ_0 varies as much as 45 dB in relatively calm sea conditions as the grazing angle changes from 0.1 to 1°. The strong dependence of clutter power on sea surface reflectivity, and hence grazing angle, is a motivation to incorporate all incident angles into the clutter model.

III. Angular Spectral Estimation

Angular spectral estimation techniques find the incident power distribution versus grazing angle. The elements of the vertical synthetic array are formed from the complex field u at each range obtained from the FFT bins of the electromagnetic parabolic equation (PE) propagation model. For Cartesian coordinates [8]

$$u(x,z) = e^{-jkx}\psi(x,z) \tag{5}$$

where x is the horizontal Cartesian range, z is the altitude, and k is the wavenumber. ψ is the tangential electric field E_y for horizontal polarization, and the tangential magnetic field H_y for vertical polarization.

The maximum inter-element spacing of the synthetic array Δz is derived from the aliasing criterion in the parabolic equation model [8]

$$\Delta z \leq \frac{\lambda}{2\sin(\alpha_{\max})}. \tag{6}$$

where $\alpha_{\max}$ is the cone angle of the valid parabolic equation approximation to the full field (see Section V). Assuming plane wave propagation, the required number of array elements N_a to achieve the desired null-to-null beamwidth $\theta_{\rm BW}$ according to the Rayleigh resolution limit is expressed as [23]

$$N_a = \frac{\lambda}{\Delta z \theta_{\rm BW}/2}. \tag{7}$$

To find the angular spectral distribution of the incoming electromagnetic wavefronts, the elements of each synthetic array should be properly phase shifted and added coherently. One important assumption in the angular spectral distribution methods for finding the grazing angle is that the PE approximation should be valid for the full field.

Curved wave spectral estimation (CWS) is discussed next, followed by a summary of plane wave spectral estimation (PWS) as a special case of CWS. Curved wave spectral estimation handles curvature in wavefronts due to an inhomogenous medium. It is demonstrated that unlike PWS, CWS produces comparable results with ray theory irrespective of the refractivity gradient.

A. Wentzel–Kramers–Brillouin–Jeffreys Approximation to Wave Propagation

The flat earth approximation is a modification to the atmospheric refractive index n_r which is equivalent to transforming the spherical propagation problem into a horizontal propagation one:

$$n_{\rm mod} = n_r + \frac{z}{r_e} \tag{8}$$

where $n_{\rm mod}$ is the modified refractive index and r_e is the radius of the Earth. Pekeris has shown that this transform often can be used for distances of up to half the Earth radius without incurring an error of more than 2% at any frequency [1]. The modified refractivity, M, is the part per million deviation from the refractivity index of a vacuum, defined as

$$M = (n_{\rm mod} - 1) \times 10^6. \tag{9}$$

The Wentzel–Kramers–Brillouin–Jeffreys (WKBJ) approximation provides a locally plane wave solution in a lossless inhomogeneous medium assuming that the field solution $u(x,z)$ is separable: $u(x,z) = t(x)f(z)$. This approximation requires vertical variations of the vertical wavenumber $k_v(z)$ to be [24]

$$\left|\frac{dk_v}{dz}\right| \ll \frac{k_v^2}{2\pi}. \tag{10}$$

The latter condition can be simplified in locally plane wave propagation to the condition that the medium should change slowly with respect to the wavelength. Similar conditions should hold as the wavenumber changes across the x direction. Vertical and horizontal refractivity index variations in almost all atmospheric conditions, including ducting situations, satisfy the aforementioned conditions. Hence, CWS is applicable to all practical cases in lower atmospheric propagation.

The vertical field $h(z)$ for one pair of incident and reflected wavefronts in the WKBJ solution is expressed as [24]

$$h(z,\theta) = \frac{A_i}{\sqrt{k_v(z,\theta)}} e^{+j\int_{z_1}^{z} k_v(z,\theta)dz} + \frac{A_r}{\sqrt{k_v(z,\theta)}} e^{-j\int_{z_1}^{z} k_v(z,\theta)dz} \tag{11}$$

where A_i and A_r are constants of the incident and forward reflected fields, and z_1 denotes the sea surface. A_i and A_r are related by $A_r = \Gamma A_i$, where Γ is the forward reflection coefficient. The total vertical field $f(z)$ is a summation over multiple pairs of incident and reflected wavefronts at each range.

To find the surface reflection coefficient Γ in (11), we apply the Kirchoff approximation and model the effect of a rough sea surface. Based on the Miller–Brown–Vegh (MBV) model [25], an effective surface reflection coefficient can be expressed as a reduction ρ to the smooth surface Fresnel reflection coefficient Γ_0

$$\gamma_w(\theta) = \frac{2\pi}{\lambda} h_w \sin\theta, \tag{12}$$

$$\rho(\theta) = e^{-2\gamma_w^2(\theta)} I_0\left[2\gamma_w^2(\theta)\right], \tag{13}$$

$$\Gamma(\theta) = \rho(\theta)\Gamma_0. \tag{14}$$

Assuming an infinite sea surface impedance for both vertical and horizontal polarizations is a good approximation at microwave frequencies and small grazing angles [8]. Thus, $\Gamma_0 = -1$ for the field u. Above, I_0 is the modified Bessel function of the first kind, and h_w is the rms wave height from the Phillips ocean wave spectrum [26]:

$$h_w = 0.0051 v_w^2 \tag{15}$$

where v_w is the wind speed in m/s. Computing Γ by (12)–(14) has been reported to agree well with measurements when $\gamma_w < 1.8$ [25], [27].

An incident wavefront with wavenumber $k(z) = (\omega)/(c(z)) = (\omega n_{\rm mod(z)})/(c_0)$ arrives at height z with horizontal angle θ_z, angular frequency ω, and wave speed $c(z)$; c_0 is the electromagnetic wave speed in a vacuum. The horizontal wavenumber k_h is constant due to Snell's law

$$k_h(z,\theta) = k(z)\cos\theta_z = k(z_1)\cos\theta \tag{16}$$

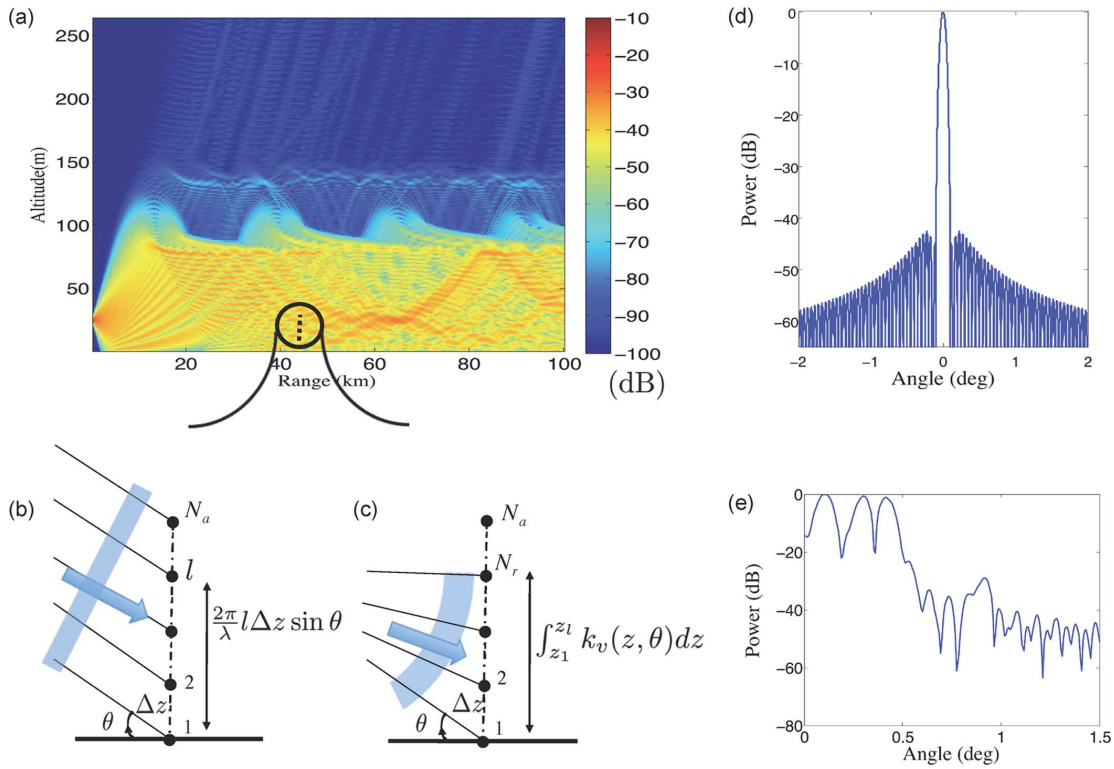

Fig. 2. (a) Power $|u|^2$ (dB) from PE in an arbitrary surface-based duct. (b),(c) Geometry of the line array used for the estimation of grazing angles at each range for plane and curved wave spectral estimation. (d) The spatial transfer function of a 200 element Hamming window with inter-element spacing of 5.7λ. (e) Normalized angular power spectrum $|B_{\mathrm{CWS},1}(\theta)|^2$ for an arbitrary range (65 km) of Panel (a).

where θ is the grazing angle at the surface. Hence, the vertical wavenumber is

$$k_v(z,\theta) = \sqrt{k^2(z) - k_h^2(z,\theta)} = \frac{\omega}{c_0}\sqrt{n^2_{\mathrm{mod}}(z) - n^2_{\mathrm{mod}}(z_1)\cos^2\theta}. \quad (17)$$

Vertical phase changes of the field are obtained by integration over the vertical wavenumber.

B. Curved Wave Spectral Estimation

Consider the geometry in Fig. 2. Panel (a) shows the power diagram $|u|^2$ for an arbitrary antenna setting and a surface-based duct. Panels (b) and (c) show linear synthetic arrays along the z-axis with equal inter-element spacing Δz similar to the height grid size in the parabolic equation model.

Curved wave spectral estimation (CWS) is a method of non-planar angular spectral estimation that matches to the curvature of waves imposed by a variable refractivity index. This method is based on the WKBJ approximation to the electromagnetic wave propagation solution. An attempt to compensate for such curvature is derived in [28], where the reference point for phase shifts is chosen at the array element with minimum wave speed. Since the grazing angle at the sea surface is of interest, the reference point here is at the sea surface z_1. The geometry of CWS is similar to that of PWS with phase differences between array elements that are calculated by integration over the vertical wavenumber.

There are two assumptions in CWS: (1) the curvature of wavefronts is only due to vertical variation in refractivity, and (2) the refractivity index of the environment varies slowly with range. Two curved wave angular estimation equations are derived. The first only matches to incident wavefronts (denoted by $B_{\mathrm{CWS},1}$), and the second matches both to incident and reflected wavefronts and yields a higher angular resolution (denoted by $B_{\mathrm{CWS},2}$).

Assume that $\{u_l\}_{l=1}^{N_r}$ are N_r samples of the field obtained from a parabolic equation approximation to the electromagnetic wave propagation. N_r is the index of the last array element with k_v real, and it is upper bounded by N_a in (7). The phase difference between the reference and lth elements located at z_1 and z_l is obtained by integration of k_v along the vertical line joining the aforementioned points

$$\phi_l(\theta) = \int_{z_1}^{z_l} k_v(z,\theta)dz. \quad (18)$$

The CWS output in direction θ is obtained by matching to the phase changes of the incident wavefront, seen in (11), assuming a grazing angle θ at the sea surface

$$B_{\mathrm{CWS},1}(\theta) = \sum_{l=1}^{N_r} w_l u_l e^{-j\phi_l(\theta)} \quad (19)$$

where $l = 1$ corresponds to the array element index at the sea surface, u_l is the complex field at the lth element of the array

obtained from the PE solution to the wave equation, and w_l is the corresponding window or shading coefficients. A Hamming window is used in this study as $\{w_l\}_{l=1}^{N_r}$ to weight array elements. The spatial transfer function of a Hamming window with 200 elements is shown in Fig. 2(d). Panel (e) shows the angular power spectrum as a function of grazing angle for an arbitrary range (65 km) of the example in Panel (a).

Using the field in the form of (11) for one pair of incident and reflected wavefronts, curved wave spectral estimation can be revised to match their sum for grazing angle θ

$$B_{\mathrm{CWS},2}(\theta) = \sum_{l=1}^{N_r} w_l u_l \left(e^{-j\phi_l(\theta)} + \Gamma(\theta) e^{j\phi_l(\theta)} \right) \qquad (20)$$

The synthetic array used in (20) is equivalent to using an array of twice the aperture where the lower half of the array virtually covers the reflected wavefront. Here we use half the Hamming window with maximum coefficient of 1 at the sea surface $(l = 1)$ for $\{w_l\}_{l=1}^{N_r}$ in (20). This window is equivalent to a full Hamming window on the equivalent synthetic array of twice the aperture. Strictly speaking, using this window is appropriate only when $\Gamma = -1$. However, it yields satisfactory results for our examples. If $\Gamma(\theta)$ is uncertain or significantly different than -1 (high wind speeds and high frequencies), (19) is better to use to estimate the incident wavefront grazing angle.

C. Plane Wave Spectral Estimation

Classical angular spectral estimation assumes plane wave propagation with a constant wave speed along the array. Plane and curved wave propagation are compared in Fig. 2(b) and (c). Plane wave spectral estimation is a special case of curved wave spectral estimation. Assuming a constant vertical wavenumber, (18) yields a constant phase advance of $(2\pi)/(\lambda)\Delta z \sin\theta$ between adjacent array elements with grazing angle θ. Thus, (19) becomes

$$B_{\mathrm{PWS},1}(\theta) = \sum_{l=0}^{N_a-1} w_l u_l e^{-j\frac{2\pi l}{\lambda}\Delta z \sin\theta} \qquad (21)$$

where an aperture of N_a elements is considered. Matching to both incident and reflected wavefronts with grazing angle θ and a constant vertical wavenumber yields an expression similar to (20)

$$B_{\mathrm{PWS},2}(\theta) = \sum_{l=0}^{N_a-1} w_l u_l \left(e^{-j\frac{2\pi l}{\lambda}\Delta z \sin\theta} + \Gamma(\theta) e^{j\frac{2\pi l}{\lambda}\Delta z \sin\theta} \right) \qquad (22)$$

where u_l and w_l are identical to those in CWS.

It has been shown that the assumption of plane wave propagation does not yield correct grazing angles comparable to ray tracing for an evaporation duct [12]. This is because the severe gradient and curvature of refractivity within the immediate vicinity of the sea-surface violates the assumption of plane wave propagation. CWS is intended to correct for this propagation curvature.

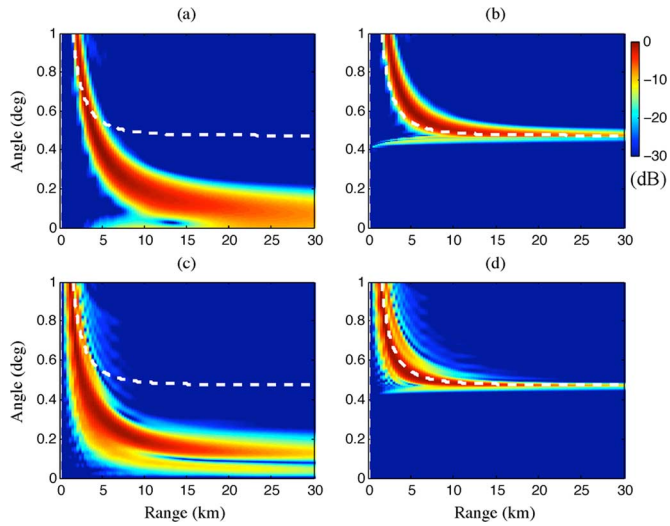

Fig. 3. Angular power spectrum for a 24 m evaporation duct, antenna height of 25 m at 10 GHz, using: (a) plane wave spectral estimation $|B_{\mathrm{PWS},1}|^2$ (21), (b) curved wave spectral estimation $|B_{\mathrm{CWS},1}|^2$ (19), (c) $|B_{\mathrm{PWS},2}|^2$ (22), (d) $|B_{\mathrm{CWS},2}|^2$ (20). Dashed lines are grazing angles obtained from the ray theory. Higher angular resolution is obtained when both incident and reflected wavefronts are considered. In each case, the angular power spectrum is normalized by the maximum power over the whole range.

Fig. 3 shows the angular spectrum obtained using plane and curved wavefront assumptions. An evaporation duct is considered with duct height of 24 m, antenna height of 25 m, frequency of 10 GHz, and wind speed of 5 m/s. As expected, better angular resolution is obtained when both incident and reflected wavefronts are considered as opposed to considering only the incident wavefront.

Fig. 4 compares the performance of ray tracing, MUSIC, PWS (22) and CWS (20) to obtain grazing angles in an evaporation duct and antenna setting identical to those of Fig. 3. Panels (a) and (b) compare angular spectral estimation for wind speed of 5 m/s at 3 and 10 GHz, respectively. The aperture is fixed at 20 m for PWS and CWS for both frequencies. The MUSIC results are obtained from Temper [9]. Note that Temper uses ray tracing in the first 3 km even in its sole MUSIC mode for grazing angle calculation. Although both MUSIC and PWS are based on the plane wave propagation assumption, the MUSIC implementation in Temper is based on dividing the synthetic array into overlapping sub-arrays. Hence, a different set of grazing angles is obtained when the refractivity index varies considerably along the array.

Previous studies on evaporation ducts showed that grazing angles obtained by ray tracing and M-layer [29] converge to the same value in the microwave region [30]. M-layer is a computer code that finds propagating modes of radio waves in a stratified atmosphere above the sea surface. Fig. 4 shows the general agreement of grazing angles obtained from ray tracing and CWS. The disagreement of CWS and ray tracing at short ranges is due to the poor approximation of PE to the total field and spherical wavefronts coming from the source. CWS assumes the

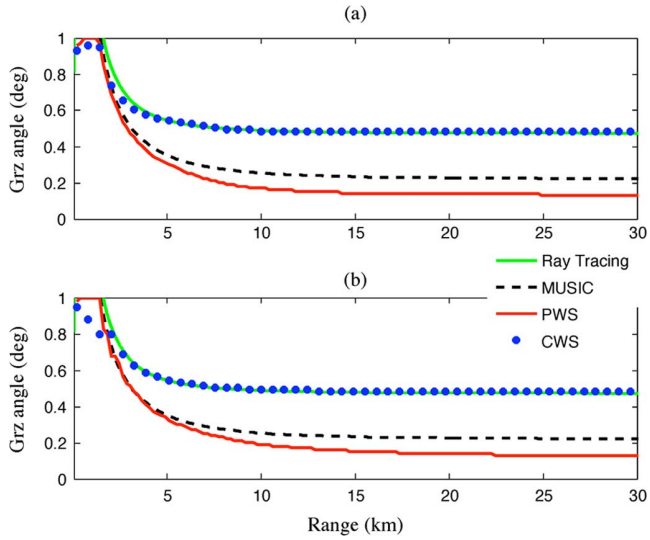

Fig. 4. Grazing angle computed by ray tracing, MUSIC, PWS and CWS for an evaporation duct with duct height of 24 m and antenna height of 25 m at (a) 3 GHz, (b) 10 GHz. The synthetic aperture is 20 m for all cases.

curvature of the wavefronts to be only due to a variable refractivity structure. This assumption breaks down near the antenna where spherical propagation dominates due to near field effects.

The disagreement between ray tracing (geometrical optics) and the plane wave propagation assumption was reported in [12]. Note that better angular estimation for PWS and MUSIC can be obtained by using a shorter array with less refractivity index variations. We use (20) and (22) in our simulations due to their higher angular resolution relative to (19) and (21) respectively. However, (19) and (21) also give similar results.

IV. Multiple Grazing Angle Clutter

Ducted environments are leaky waveguides with the ocean behaving as a reflecting surface and the duct top behaving as a partially reflecting boundary. These waveguides carry more than one mode while different groups of modes interact with the surface with different equivalent grazing angles. It is shown in Fig. 1 that surface reflectivity changes up to 45 dB as grazing angle changes from 0.1 to 1° for wind speeds of less than 10 m/s. Therefore, a realistic model for sea surface clutter depends on the summation of surface reflections over all incident angles weighted by their corresponding powers.

Assume $\gamma(\theta) = |B_{\mathrm{CWS}}(\theta)|^2$ to be the angular power spectrum obtained from (19) or (20). Considering the single grazing angle clutter model (4) and weighting the clutter power along each angle θ by the normalized power $(\gamma(\theta))/(\int_\theta \gamma(\theta))$ yields the multiple angle clutter model

$$P_c(r) = \frac{\alpha_c(r)F^4(r)}{\int_\theta \gamma(\theta)d\theta} \int_\theta \frac{\sigma_{0,\mathrm{GIT}}(\theta)\sec(\theta)\gamma(\theta)}{F^4_{\mathrm{std}}(\theta)}d\theta \qquad (23)$$

where $F_{\mathrm{std}}(\theta)$ is the propagation factor of the standard atmosphere at $r'(\theta)$ from (3), and $\alpha_c(r) = (P_t G^2 \lambda^2 \theta_B c\tau)/(2(4\pi r)^3 L)$ includes all the terms independent of θ. It has been suggested to use propagation factors at the height of 1 m to avoid cancellation of the total field at the conductor surface [4]. However, that choice of the propagation factor may lead to an error in the calculation of the clutter power. This error is negligible in most practical situations [31].

The procedure to compute the clutter power for a given refractivity profile is summarized below. Sea surface reflectivity equations are provided in Appendix A.

1) Run a parabolic equation model to obtain the field $u(x, z)$ for the desired range extent and given environment. The inter-element spacing is obtained from (6), and the number of array elements is obtained from (7).
2) For each range, construct a vertical synthetic array from the PE FFT bins.
3) Using (12)–(14) find the surface reflection coefficient $\Gamma(\theta)$ for all angles. Then, use (18) and (20) to obtain the angular distribution.
4) Use (2), (A.27) or (A.28) depending on the polarization to obtain sea surface reflectivity values for different grazing angles.
5) Calculate the total clutter power by (23) which uses the angular power spectrum and sea surface reflectivities from Steps 2 and 3.

V. Examples

Electromagnetic wave propagation examples in different ducting environments are considered here. The simulated radar in the examples operates at 3 and 10 GHz, vertically polarized with elevation angle of 0° and half-power beamwidth of 0.4°. The radar antenna is located 25 m above the sea surface and wind speed is 5 m/s.

The clutter powers due to both single and multiple grazing angle models are normalized to the power at the range of 10 km (except the example of the evaporation duct which is normalized at 5 km), so that clutter power changes of different models can be compared conveniently. For the multiple grazing angle model in (23), we use (20) for CWS and (22) for PWS due to their higher angular resolutions relative to (19) and (21), respectively. However, the latter also gives similar results.

The parabolic equation yields valid solutions for wave propagation inside a cone with vertex angle $\alpha_{\max}$ [8], here $\alpha_{\max} = 5°$. This angle is a trade-off between PE stability and accuracy. The complex field (PE solution), ray tracing results and maximum ray tracing clutter calculations are obtained from APM [7]. APM is a hybrid model that consists of four sub-models: flat earth, ray optics, extended optics, and the split-step PE model. The PE model within APM is the primary model from which all other sub-models are driven [7]. All examples described in this section are based on executing only the PE algorithm within APM. The forward scattered field of APM is obtained by using maximum angle of ray traces for surface impedance calculations at each range, i.e., the spectral method described here has not been used.

APM also computes clutter based on the modified GIT reflectivity model described in Section II.A. For over-water propagation paths, such as the examples presented in this section, APM determines the grazing angle based on ray tracing. It performs a combination of interpolation and elimination to determine the maximum grazing angle over a given range for those

cases where ducting is present and grazing angles determined by ray tracing will result in "multi-valued" grazing angles for a particular range interval. The maximum grazing angles determined from ray tracing, and used within APM for clutter computations are shown for an example in Fig. 8(c).

The theoretical bound (6) yields $\Delta z \leq 0.172$ m for 10 GHz and $\Delta z \leq 0.573$ for 3 GHz. The upper bounds are used here in each case. The CWS output is restricted to grazing angles of 0 to 1.5°. A 20 m aperture is used at 10 GHz which gives a null-to-null beamwidth of 0.17° for a rectangular window. The same resolution condition requires a 67 m synthetic aperture at 3 GHz, which usually is not possible since the aperture is limited by the duct height in this work.

A. Evaporation Ducts

Evaporation ducts are the most common types of non-standard atmospheric phenomena in maritime environments. The Paulus–Jeske model provides a relationship between modified refractivity M, altitude z and duct height h_d [32]. Assuming equal temperature of the sea surface and air layer boundary simplifies the Paulus–Jeske model [30]

$$M(z) = M_0 + c_0 \left(z - h_d \ln \frac{z + h_0}{h_0} \right) \tag{24}$$

where M_0 is the base refractivity usually taken as 300 M-units, $c_0 = 0.13$ M-unit/m is the linear slope of the refractivity and h_0 is the roughness factor taken as 1.5×10^{-4} m.

Fig. 5 compares the output power of CWS, $\gamma(\theta)$, and grazing angles computed by ray tracing for different ranges in an evaporation duct with duct height of 24 m and operational frequency of 10 GHz. The radar is located at 25 m from the sea surface. Calculated clutter power obtained from different methods also is shown.

Panel (a) shows the refractivity profile similar to [12] where MUSIC [10] was reported to fail capturing the correct grazing angles. Panel (b) shows the propagation factor, in dB, of the environment with radar conditions as described before. Panel (c) shows the angular power spectrum of CWS overlaid with grazing angles obtained from ray tracing. It shows that the peaks of CWS coincide with the ray tracing results.

CWS is performed on the PE complex field with an array of size 20 m and inter-element spacing of $\Delta z = 0.17$ m. Agreement of CWS and ray tracing is clear in Fig. 5(c). Panel (d) shows the clutter power obtained from a single grazing angle using maximum ray tracing and the multiple grazing angle model using CWS and PWS. Single angle ray tracing and multiple angle CWS result in similar clutter patterns due to the single grazing angle nature of evaporation ducts. The multiple grazing angle model that utilizes PWS has a different rate of fall-off. This will result in erroneous duct height estimation in inversion problems since the rate of fall-off of the clutter power is a function of duct height in evaporation ducts [2].

The reliability of CWS is tied to the reliability of the field calculated by PE. Fig. 5 shows that angular spectral estimation yields comparable results to ray tracing where PE is a valid approximation to the full field and curved wavefronts are not due to near field spherical propagation.

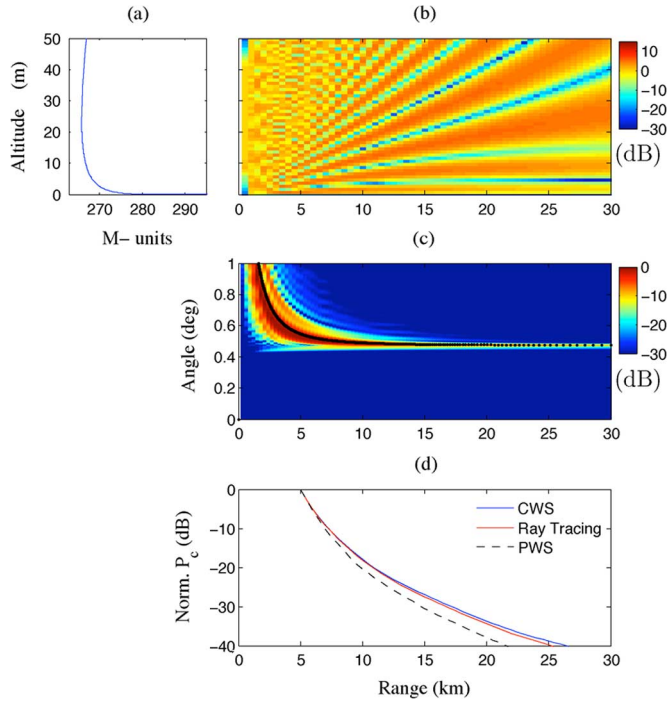

Fig. 5. (a) M-profile of an evaporation duct with $h_d = 24$ m. (b) Propagation factor F in dB for 10 GHz. (c) Output power of CWS normalized by the maximum power over the whole range, compared to the grazing angle computed by ray tracing (solid). (d) Clutter power calculated by maximum ray tracing and the multiple grazing angle model (CWS, PWS).

B. Surface-Based Ducts

Surface ducts occur when humidity and temperature inversions are both present which typically is due to the advection of warm and dry coastal air to the sea. These ducts are less common than evaporation ducts but their effect is more prominent on radar returns [1]. The M-profile of a range-independent surface based duct can be approximated by a bilinear or tri-linear function (depending on the structure of the refractivity profile)

$$M(z) = M_0 + \begin{cases} c_1 z & z \leq h_1 \\ c_1 h_1 + c_2 (z - h_1) & h_1 \leq z \leq h_2 \\ c_1 h_1 + c_2 h_2 & h_2 \leq z \\ \quad +0.118(z - h_1 - h_2). & \end{cases} \tag{25}$$

Refractivity changes along the array in the examples shown in Figs. 6–8 are small such that curvature of wavefronts along the array is negligible. Hence, MUSIC and CWS will obtain similar angles. Fig. 6 shows an example of a surface based duct taken from [12] with radar frequency of 10 GHz and antenna height 25 m to show the agreement of CWS with previous studies. As used in [12], MUSIC with forward/backward smoothing [11] assumes a constant refractivity index by averaging over overlapping sub-arrays. The panels are similar to those of Fig. 5.

Ray tracing does not always result in smooth variations of calculated grazing angles. Fig. 7(a) is an example where ray tracing results in discontinuities while CWS results in smooth grazing angle estimation without any further processing and extra assumptions. This continuity results in a continuos clutter power, as seen in Fig. 7(b). The refractivity profile and radar conditions

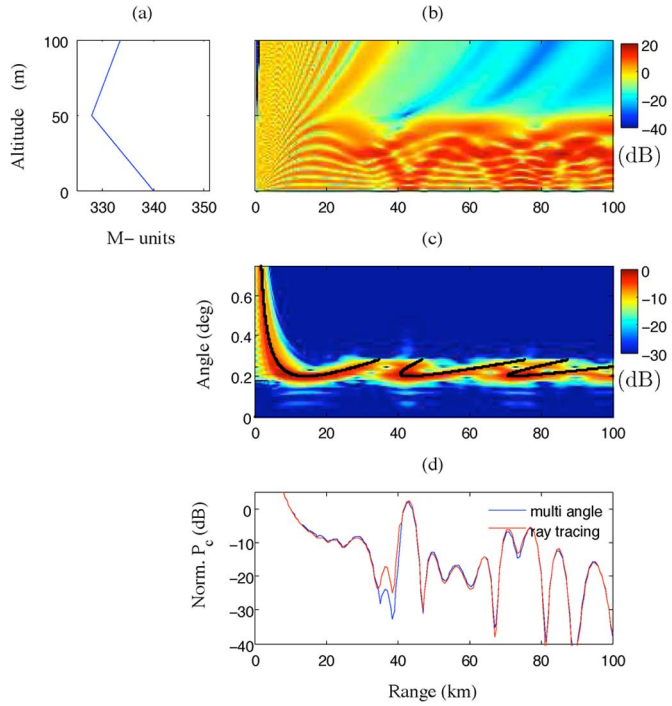

Fig. 6. (a) M-profile of a surface-based duct. (b) Propagation factor F in dB for 10 GHz. (c) CWS output power normalized by the maximum power over the whole range, overlaid with grazing angles obtained from ray tracing (solid). (d) Clutter power from maximum ray tracing and the multiple grazing angle model.

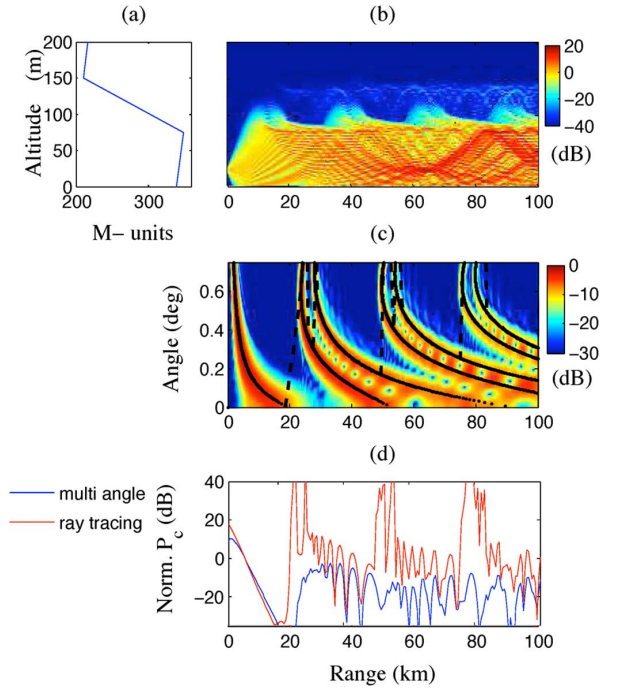

Fig. 8. (a) M-profile of a surface-based duct. (b) Propagation factor F in dB for 10 GHz. (c) CWS output power normalized by the maximum power over the whole range, overlaid with grazing angles obtained from ray tracing (solid) and maximum of ray traces (dashed). (d) Clutter power from maximum ray tracing and the multiple grazing angle model based on CWS.

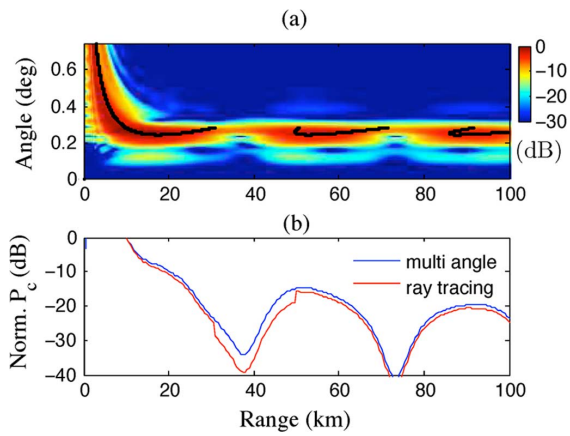

Fig. 7. Discontinuity in clutter power when grazing angle is obtained from ray tracing. Similar refractivity profile and conditions as in Fig. 6 except that antenna height and frequency are 45 m and 3 GHz. (a) CWS output power normalized by the maximum power over the whole range, overlaid with grazing angle obtained from ray tracing (solid). (b) Multiple angle clutter power based on CWS and single angle clutter based on ray tracing.

are all similar to Fig. 6 except that the operational frequency is at 3 GHz and antenna height is 45 m. Interpolation methods such as greatest angle path (GAP) have been developed that yield relatively continuous grazing angles biased toward larger ray trace angles [13]. However, these methods were developed to keep the single grazing angle smooth and are not necessarily correct physically.

An example of multiple arrivals with comparable power is provided in Fig. 8 where a surface-based duct is used with the refractivity profile shown in Panel (a). All radar simulation parameters are similar to the other examples. Using only one of the ray traces as the grazing angle is not representative of the incident wave. However, angular spectral estimation captures all incident angles and their corresponding relative powers. Panel (c) shows that multiple grazing angles are present where none is dominant. Using the maximum grazing angle may result in an unrealistic dynamic range of the clutter power, as observed in Panel (d).

C. *SPANDAR 1998 Measured Refractivity*

A refractivity profile measured during the Space Range Radar (SPANDAR) experiment, Wallops Island, Virginia, April 2, 1998 [15], [30] is considered here. This profile was measured using an instrumented helicopter provided by the Johns Hopkins University Applied Physics Laboratory. The particular refractivity profile used here is from Run 07, at a range of 59 km from the SPANDAR.

Fig. 9 is an example using real refractivity profile measurements that shows agreement of angular spectral estimation using CWS and grazing angles obtained from ray theory.

VI. Conclusion

A multiple grazing angle clutter model based on curved wave spectral estimation (CWS) has been introduced. CWS is a generalization of plane wave spectral estimation (PWS) where curvature of wavefronts due to changes in the refractivity index is considered. Examples demonstrated that the power versus grazing angle obtained by CWS is more accurate than PWS and

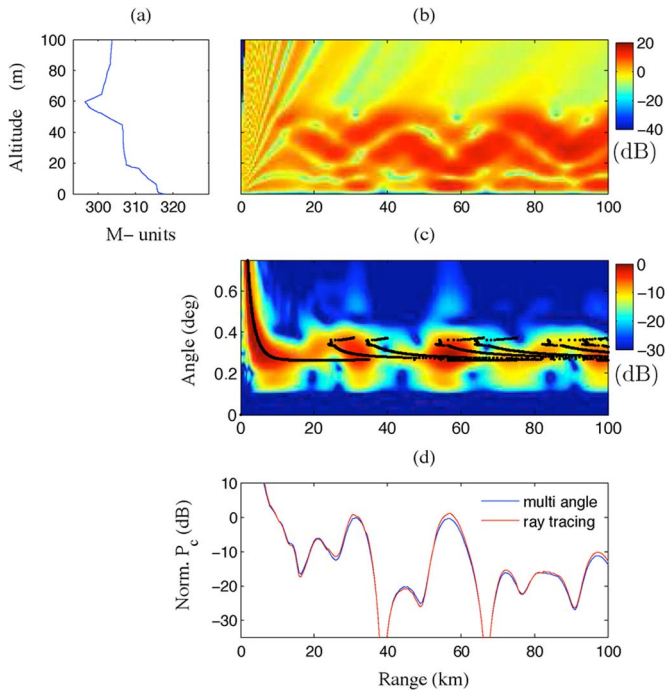

Fig. 9. (a) M-profile measured during the SPANDAR 1998 experiment. (b) Propagation factor F in dB for 3 GHz. (c) CWS output power normalized by the maximum power over the whole range, overlaid with grazing angles obtained from ray tracing (dark line). (d) Clutter power from maximum ray tracing and the multiple grazing angle model.

it does not have the problem of discontinuity in grazing angles introduced by ray tracing.

The multiple grazing angle clutter model integrates over all grazing angles weighted by the angular power spectrum. Grazing angles can be determined by CWS from a synthetic vertical array generated by samples of the field. These samples are obtained from a parabolic equation propagation model. The performance of this clutter model was compared to that of single grazing angle clutter calculations for evaporation and surface-based ducts. This method yields a more realistic model for the received clutter that then can be used in estimation of the refractivity profile of the ambient environment based on the observed backscattered radar signal. Although the multiple grazing angle clutter model has been derived for sea clutter, it also can be adapted for land clutter.

Appendix A
GIT Model

Sea surface reflectivity computation in this work is based on the Georgia Institute of Technology (GIT) model [3]. Reilly and Dockery modified the GIT model to incorporate the atmospheric condition influence on the sea surface reflectivity [4], [5], [22].

The basic GIT model calculates the sea surface reflectivity per unit area of vertical and horizontal polarizations by considering an average wave height in a given sea condition and taking into account the radar look direction [3]

$$h_{\rm av} = 0.00425 v_w^{2.5} \tag{A.26}$$

where $h_{\rm av}$ is the average wave height in meters, and v_w is the wind speed in m/s. Defining

$$a = (14.4\lambda + 5.5)\theta \frac{h_{\rm av}}{\lambda}$$
$$q = 1.1(\lambda + 0.015)^{0.4}$$

in which λ is the wavelength in meters, and θ is the grazing angle in radians. Then

$$G_a = \frac{a^4}{a^4 + 1}$$
$$G_M = \exp\left\{0.2(1 - 2.8\theta)(\lambda + 0.015)^{-0.4}\cos\psi\right\}$$
$$G_w = \left(\frac{1.94 v_w}{1 + v_w/15.4}\right)^q$$

where ψ is the angle between the antenna look direction and the wind direction. The GIT sea surface reflectivity model is

$$\sigma_{0h,\rm GIT} = 10\log\left(3.9\times 10^{-6}\lambda\theta^{0.4} G_a G_M G_w\right) \tag{A.27}$$

$$\sigma_{0v,\rm GIT} = \begin{cases} \sigma_{0h,\rm GIT} - 1.73\ln(h_{\rm av} + 0.015) \\ \quad +3.76\ln(\lambda) + 2.46\ln(\theta + 0.0001) \\ \quad +22.2 \qquad 1 \text{ to } 3 \text{ GHz} \\ \sigma_{0h,\rm GIT} - 1.05\ln(h_{\rm av} + 0.015) \\ \quad +1.09\ln(\lambda) + 1.27\ln(\theta + 0.0001) \\ \quad +9.70 \qquad 3 \text{ to } 10 \text{ GHz} \end{cases} \tag{A.28}$$

where $\sigma_{0h,\rm GIT}$ and $\sigma_{0v,\rm GIT}$ are the sea surface reflectivities per unit area for H and V polarizations obtained from the GIT model, in dB. The effect of the angle between the radar look direction and wind direction is an additive bias term as $\cos\psi$ in the sea surface reflectivity.

References

[1] M. I. Skolnik, *Radar Handbook*, 3rd ed. New York: McGraw-Hill, 2008.

[2] C. Yardim, P. Gerstoft, and W. S. Hodgkiss, "Sensitivity analysis and performance estimation of refractivity from clutter technique," *Radio Sci.*, vol. 44, no. RS1008, 2009, doi:10.1029/2008RS003897.

[3] M. Horst, F. Dyer, and M. Tuley, "Radar sea clutter model," in *Proc. Int. Inst. Elect. Eng. Antennas Propagation Society/URSI Symp.*, London, England, Nov. 1978, pp. 6–10.

[4] G. D. Dockery, "Method for modeling sea surface clutter in complicated propagation environments," *IEE Proc. Radar Signal Processing*, vol. 137, pp. 73–79, 1990.

[5] J. P. Reilly and G. D. Dockery, "Influence of evaporation ducts on radar sea return," *IEE Proc. Radar Signal Processing*, vol. 137, pp. 80–88, 1990.

[6] V. Gregers-Hansen and R. Mital, "An empirical sea clutter model for low grazing angles," in *Proc. IEEE Radar Conf.*, Pasadena, CA, May 2009, pp. 1–5.

[7] A. E. Barrios, "Advanced propagation model (APM) computer software configuration item (CSCI)," Space and Naval Warfare Systems Center, TD 3145, Aug. 2002.

[8] M. Levy, *Parabolic Equation Methods for Electromagnetic Wave Propagation*. London: Inst. Elect. Eng., 2000.
[9] G. D. Dockery, "Modeling electromagnetic wave propagation in the troposphere using the parabolic equation," *IEEE Trans. Antennas Propag.*, vol. 36, no. 10, pp. 1464–1470, 1988.
[10] R. O. Schmidt, "Multiple emitter location and signal parameter estimation," *IEEE Trans. Antennas Propag.*, vol. 34, no. 3, pp. 276–280, 1986.
[11] S. U. Pillai and B. H. Kwon, "Forward/backward spatial smoothing techniques for coherent signal identification," *IEEE Trans. Acoust. Speech Signal Process.*, vol. 37, no. 1, pp. 8–15, Jan. 1989.
[12] G. D. Dockery and J. R. Kuttler, "An improved impedance-boundary algorithm for Fourier split-step solution of the parabolic wave equation," *IEEE Trans. Antennas Propag.*, vol. 44, no. 12, pp. 1592–1599, 1996.
[13] G. D. Dockery, R. S. Awadallah, D. E. Freund, J. Z. Gehman, and M. H. Newkirk, "An overview of recent advances for the TEMPER radar propagation model," in *Proc. IEEE Radar Conf.*, Apr. 2007, pp. 896–905.
[14] R. Janaswamy, "Radio wave propagation over a nonconstant immittance plane," *Radio Sci.*, vol. 36, pp. 387–405, May–Jun. 2001.
[15] P. Gerstoft, L. T. Rogers, J. L. Krolik, and W. S. Hodgkiss, "Inversion for refractivity parameters from radar sea clutter," *Radio Sci.*, vol. 38, no. 3, pp. 1–22, Apr. 2003, doi:10.1029/2002RS002640.
[16] P. Gerstoft, L. T. Rogers, W. S. Hodgkiss, and L. J. Wagner, "Refractivity estimation using multiple elevation angles," *IEEE J. Ocean. Eng.*, vol. 28, pp. 513–525, Jul. 2003.
[17] C. Yardim, P. Gerstoft, and W. S. Hodgkiss, "Estimation of radio refractivity from radar clutter using Bayesian monte Carlo analysis," *IEEE Trans. Antennas Propag.*, vol. 54, no. 4, pp. 1318–1327, 2006.
[18] S. Vasudevan, R. Anderson, S. Kraut, P. Gerstoft, L. T. Rogers, and J. L. Krolik, "Recursive Bayesian electromagnetic refractivity estimation from radar sea clutter," *Radio Sci.*, vol. 42, no. RS2014, 2007, doi:10.1029/2005RS003423.
[19] C. Yardim, P. Gerstoft, and W. S. Hodgkiss, "Tracking refractivity from clutter using Kalman and particle filters," *IEEE Trans. Antennas Propag.*, vol. 56, no. 4, pp. 1058–1070, 2008.
[20] A. Karimian, C. Yardim, P. Gerstoft, W. S. Hodgkiss, and A. E. Barrios, "Refractivity estimation from sea clutter: An invited review," *Radio Sci.*, vol. 46, no. RS6013, 2011, doi:10.1029/2011RS004818.
[21] A. Karimian, C. Yardim, P. Gerstoft, W. S. Hodgkiss, and A. E. Barrios, "Estimation of refractivity using a multiple angle clutter model," *Radio Sci.*, 2012, to be published.
[22] J. P. Reilly and G. D. Dockery, Calculation of Radar Sea Return With Consideration of Propagation Conditions NATO, AAW Tech. Rep. NNW-88-141, Dec. 1988.
[23] H. L. VanTrees, *Optimum Array Processing*. New York: Wiley, 2002.
[24] C. G. Someda, *Electromagnetic Waves*, 2nd ed. London, U.K.: Taylor and Francis Group, 2006.
[25] A. R. Miller, R. M. Brown, and E. Vegh, "New derivation for the rough surface reflection coefficient and for the distribution of the sea-wave elevations," in *Proc. Inst. Elect. Eng., pt. H*, Apr. 1984, vol. 131, no. 2, pp. 114–116.
[26] O. M. Phillips, "Spectral and statistical properties of the equilibrium range in wind-generated gravity waves," *J. Fluid. Mech.*, vol. 156, pp. 505–531, 1985.
[27] D. E. Barrick, "Grazing behavior of scatter and propagation above any rough surface," *IEEE Trans. Antennas Propag.*, vol. 46, no. 1, pp. 73–83, 1998.
[28] M. Dzieciuch, P. Worcester, and W. Munk, "Turning point filters: Analysis of sound propagation on a gyre-scale," *J. Acoust. Soc. Am.*, vol. 110, no. 1, pp. 135–149, 2001.
[29] H. M. Lee and Y. Y. Han, "M-layer: NPS version," *IEEE Trans. Magn.*, vol. 29, no. 2, pp. 1363–1367, 1993.
[30] L. T. Rogers, C. P. Hattan, and J. K. Stapleton, "Estimating evaporation duct heights from radar sea echo," *Radio Sci.*, vol. 35, no. 4, pp. 955–966, 2000.
[31] G. C. Konstanzer, J. Z. Gehman, M. H. Newkirk, and G. D. Dockery, "Calculation of the surface incident field using TEMPER for land and sea clutter modeling," in *Proc. on Low Grazing Angle Clutter: Its Characterization, Measurement and Application, RTO-MP-60*, 2000, pp. 14-1–14-2.
[32] R. A. Paulus, "Practical applications of an evaporation duct model," *Radio Sci.*, vol. 20, pp. 887–896, 1985.

Ali Karimian received the B.S. degree in electrical engineering from Sharif University of Technology, Tehran, Iran, in 2007. He is currently working toward the Ph.D. degree at the University of California, San Diego.

Since 2010, he has been a Graduate Research Associate with the Marine Physical Laboratory, University of California, San Diego. His research interests include signal processing, statistical learning, propagation and remote sensing.

Caglar Yardim (S'98–M'07) received the B.S. and M.S. degrees in electrical engineering from the Middle East Technical University, Ankara, Turkey, in 1998 and 2001, respectively, and the Ph.D. degree in electrical engineering from the University of California, San Diego, in 2007.

He is currently a Scientist at the Marine Physical Laboratory, University of California, San Diego. His research interests include signal processing, remote sensing, propagation, acoustics, electromagnetics, and seismics.

Dr. Yardim was the recipient of the Best Student Paper Award at the 2007 IEEE Radar Conference and URSI Young Scientist Award in 2008.

Peter Gerstoft received the Ph.D. degree from the Technical University of Denmark, Lyngby, Denmark, in 1986.

From 1992–1997, he was at NATO Undersea Research Centre, La Spezia, Italy. Since 1997, he has been with the Marine Physical Laboratory, University of California, San Diego. His research interests include modeling and inversion of acoustic, elastic and electromagnetic signals.

Dr. Gerstoft is a Fellow of Acoustical Society of America and an elected member of the International Union of Radio Science, Commission F.

William S. Hodgkiss (S'68–M'75) received the B.S.E.E. degree from Bucknell University, Lewisburg, PA, in 1972, and the M.S. and Ph.D. degrees in electrical engineering from Duke University, Durham, NC, in 1973 and 1975, respectively.

Since 1978, he has been a member of the faculty of the Scripps Institution of Oceanography, University of California, San Diego, and on the staff of the Marine Physical Laboratory where currently he is Deputy Director. His present research interests are in the areas of signal processing, communications, propagation modeling, ambient noise, and environmental inversions, with applications of these to underwater acoustics and electromagnetic wave propagation.

Dr. Hodgkiss is a Fellow of the Acoustical Society of America.

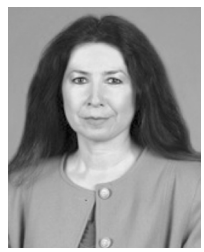

Amalia E. Barrios received the B.S. degree in physics from the California State University at Fresno, in 1983 and the M.S.E.E. degree in communication theory and systems from the University of California, San Diego, in 1989.

In 1983, she joined the Atmospheric Propagation Group in what is now the Space and Naval Warfare Systems Center Pacific, in San Diego. Since 1983, she has developed and co-developed radiowave propagation models and algorithms for use in the VHF to Q-band frequencies, accounting for anomalous propagation conditions and variable terrain.